AFRL-AFOSR-VA-TR-2019-0081

Experimental Investigation of Dynamic Flow Interactions in Shock-Induced Separated Corner Boundary Layers

Venkateswaran Narayanaswamy
NORTH CAROLINA STATE UNIVERSITY
2701 SULLIVAN DR, STE 240, CAMPUS BX 7
RALEIGH, NC 27695-7003

04/02/2019
Final Report

Air Force Research Laboratory
AF Office Of Scientific Research (AFOSR)/RTA1

Arlington, Virginia 22203
Air Force Materiel Command

Experimental Investigation of Shock Boundary Layer Interactions to Unravel Inlet Unstart Physics

Table of Contents

I. Summary of Activities 2

II. Personnel Supported 2

III. Publications and Technical Reports 2

IV. Accomplishments and New Findings 2

V. Summary of Results 3

V.A. Introduction 3

V.B. Experimental Setup 5

V.C. Results and Discussion 7

VI. Conclusions 19

VII. References 20

I. Summary of Activities

This report summarizes the activities and major findings of the AFOSR Grant dedicated to understand the shock boundary layer interactions that are relevant to rectangular inlet/isolator unstart. The objective of the proposed effort is to understand the mutual interactions between primary and corner separation units in the isolator and elucidate how they result in enhanced growth of the separated flow in isolators. Meeting this objective required a combination of experimental tools that included qualitative surface streakline visualization and quantitative wall pressure measurements along the primary and corner separation over a wide range of back pressure ratios. The separation units were generated by shock boundary layer interactions (SBLI) generated by a compression ramp placed in a Mach 2.5 flow; the back pressure ratio was varied between 2 to 4 by changing ramp angles between $12° - 24°$. The highest back pressure employed is about 60% of the normal shock value. The work focused on the following tasks:

- **Semi-quantitative mean SBLI flowfield delineation:** This task involved delineation of mean features of primary and corner separation units using surface streakline visualization and their evolution with increasing back pressure
- **Time-resolved wall pressure measurements along primary and corner SBLI:** This task involved elucidating the dynamic features of the primary and corner SBLI and their respective driving sources using time-resolved wall pressure measurements along the SBLI units. The evolution of SBLI features with increasing back pressure is also studied by obtaining the wall-pressure measurements over the different back pressure ratios.
- **Time-correlated visualization of the dynamic interactions between corner and primary SBLI:** The task involved obtaining trajectories of near-wall streaklines to delineate the fluid migration between primary and corner separation units at various back pressures to elucidate the dynamic interactions between the two separation units.

II. Personnel Supported

1. Dr. Venkat Narayanaswamy – Assistant Professor

2. Morgan Funderburk – Graduate Research Assistant

III. Publications and Technical Reports

1. Funderburk, M., and Narayanaswamy, V., **"Experimental Investigation of Primary and Corner Shock Boundary Layer Interactions at Mild Back Pressure Ratios,"** *Physics of Fluids*, Vol. 28, 086102, 2016.

2. Funderburk, M., and Narayanaswamy, V., "**Experimental Investigation of Shock Boundary Layer Interactions to Unravel Inlet Unstart Physics",** *Journal of Fluid Mechanics, Under Preparation, 2016*

3. Funderburk, M., "**Experimental Investigation of Shock Boundary Layer Interactions to Unravel Inlet Unstart Physics**", Masters Thesis, North Carolina State University, 2016.

4. Funderburk, M., and Narayanaswamy, V., "**Experimental Investigation of Shock Boundary Layer Interactions to Unravel Inlet Unstart Physics",** *AIAA Aviation Conference 2016*

IV. Accomplishments and New Findings

Prior to this study, there was very little information on the shock boundary layer interactions that occur prior to unstart initiation and during perpetuation. Some of the most basic questions like "*what mechanisms caused the spiraling growth of the separated flow? Is corner separation important in the overall isolator separated flow and if yes, what is its role in the separated flow growth during and prior to unstart?*" remained open.

Through this effort, we now have unprecedented information that provides answers to both the above questions. Our results provided unique insights into the dynamics of the primary and corner separated flows and the sources that

drive these separation units. Further our results suggest that the corner separation is indeed an integral driving unit of the separated flow dynamics of the entire isolator flow. Some of our new findings include:

1. At very mild pressures, the corner and primary separation function as independent units locally driven by incoming boundary layer and downstream separated flow instabilities.

2. With increasing back pressure, mutual interactions between the corner and primary separation units become very apparent both in streakline visualization as well as dynamic pressure fluctuation measurements. At high back pressures, the corner separation unit behaves as an interacting part of a global separation unit encompassing the entire isolator separated flow, such that both corner and primary separation units pulsate as a coupled system.

3. Time-correlated surface streakline movies show that, at high back pressures, the primary separation near-wall fluid feed the corner vortices. The fluid in primary separation unit is regenerated at the reattachment line from the near wall fluid entrainment along the side wall and probably by off-surface fluid over the primary separation shear layer.

These results show that the corner separation indeed plays a vital part in the monotonic growth of the separated flows prior to and during unstart.

V. Summary of Results

V.A. Introduction

Stabilization of oblique shock trains is a necessity within the mixed compression inlets of ramjet and scramjet type engines for successful operation. These oblique shock trains generate sufficient compression of the low density freestream flow for combustion without the excessive cowl wave drag penalty associated with external compression type inlets. However, the mixed compression inlet type suffers from an increased susceptibility to shock-induced boundary layer separation at the inlet walls and junctions between adjacent walls [1]. Separation of the wall boundary layers reduces the effective cross sectional area of the inlet resulting in a choking phenomenon, and subsequently the mass flow rate to the combustion chamber is reduced. Further, the downstream pressure rise due to heat release in the combustion chamber coupled with inlet compression can increase the adverse pressure gradient to the point that the highly sensitive shock train is ejected from the inlet entirely in an upstream sweeping motion known as unstart [2]. An unstart event is immediately followed by a drastically reduced mass flow rate through the engine, loss of thrust, and a large transient pressure loading [3]. The likelihood of such an event is exacerbated for the scramjet type engine at low flight Mach numbers; this effect severely limits the potential of future air-breathing single-stage-to-orbit (SSTO) vehicles, which require a combination of conventional turbojet and ram/scramjet modes to produce thrust from takeoff to maximum speeds well above Mach 8 [3]. By reducing the scramjet starting speed, the intermediate ramjet phase can be eliminated entirely to reduce the weight and mechanical complexity of the propulsion system. While many other significantly difficult technologies must be solved before such a vehicle can become a reality, the practical relevance of the unstart issue is not limited to future prospects. As of the time of this writing, unstart persists as a limiting factor in the flight-testing of highly experimental scramjet testbeds like the Boeing X-51 Waverider [4].

In the interest of developing eventual unstart prevention and control methodologies, many studies both experimental and computational in nature have focused on characterizing the process itself [5-13]. Early efforts to delineate the causes of mixed compression inlet unstart were primarily focused on unstart initiated by combustion-induced pressure rise due to heat release. Experiments with this aim generally consisted of rectangular inlet/isolator models, and various methods of emulating the pressure rise were implemented, such raising a flap [5, 6, 7], introducing an obstruction [8], and injecting high-momentum jets [9]. Similarly geared experiments involving the inclusion of a downstream combustor have also been performed [10, 11]. By and large, the unstart processes reported are highly similar and are thus independent of the initiating pressure rise, be it combustion-induced or emulated. The initial heat release or pressure rise is followed immediately by the establishment of the unstart shock system, typically within a few ms. Weiting [8] showed that the unstart shock system traveled at average streamwise

velocities between $1 - 4\% \, u_\infty$ in the laboratory reference frame once initiated. Next, an oscillatory motion in and out of the inlet was observed by Wagner et al. [5], followed by a non-oscillatory bulk upstream propagation of the shock system, corroborated by Do et al. [9].

While the aforementioned works agree well in their accounts of upstream-propagating unstart shock systems, they reach differing conclusions regarding the mechanisms responsible. Wagner et al. [5] suggested a strong association between the initiation of an unstart event and shock-induced wall boundary layer separation, while Laurence et al. [10] observed minimal wall boundary-layer separation, and hence concluded that local thermal choking was the more likely cause for unstart origination, an idea consistent with the earlier suppositions of O'Byrne et al. [11]. Seemingly then, there is a lack of consensus on the true initiation mechanism of inlet unstart in *steady* combustion situations, the two most likely candidates being thermal choking due to combustor heat release and shock-induced wall boundary layer separation. It should be noted that there are reported unstart events from combustion instabilities which propagate large changes in back pressure; here the overwhelming cause of unstart is indeed the shock boundary layer interactions.

Significant computational efforts were made to elucidate the distinct unstart cause in steady combustion situations. McDaniel & Edwards [12, 13] performed Reynolds-averaged Navier-Stokes (RANS) simulations on a combustor flowfield similar to that of O'Byrne et al.'s experiment. Initially, two-dimensional simulations pointed to thermal choking as the likely cause [12]. However, the later implementation of a three-dimensional domain and numerics suggested that unstart was initiated by large separated regions of the inlet wall boundary layer resulting from an impinging oblique shock wave [13]. Subsequently, blockage of the core flow occurred *before* sufficient heat had been released for thermal choking. Therefore, it seems that even in heat-release initiated unstart events, shock-induced boundary layer separation precedes thermal choking as the driving mechanism.

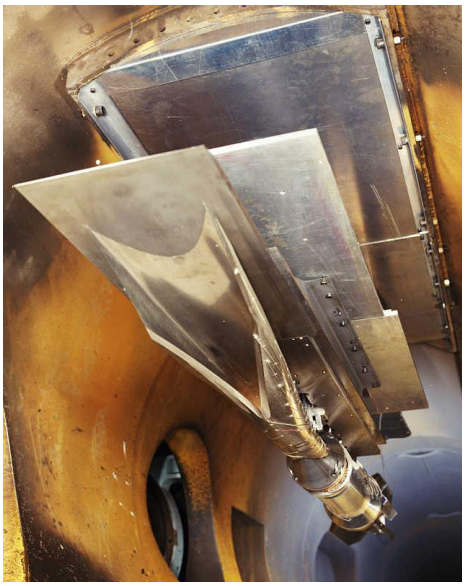

Figure 1. Experimental model of the REST type hypersonic inlet

With shock-induced wall boundary layer separation appearing to play a prominent role in the initiation of mixed compression inlet unstart, it will prove useful to review the significant body of research pertaining to canonical two-dimensional shock wave boundary layer interactions (2D SBLI). Numerous reviews capture the progress in this area over several decades [14, 15, 16, 17, 18]. While the insights they provide are certainly valuable, they are somewhat limited in their application to the mixed compression inlet, where a considerable portion of the incoming flowfield is three-dimensional (3D) in nature. Consider a proposed configuration known as the Rectangular-to-Elliptical-Shape-Transition (REST) inlet [19] depicted in Figure 1. The cross-sectional area of the REST inlet gradually evolves from an upstream rectangular shape (which allows the side-to-side placement of inlets on multi-engine vehicles) to an ellipse, allowing for utilization of an elliptical combustor. At the junctions of the upstream inlet walls, highly three-dimensional corner boundary layers are formed. These boundary layers are characterized by streamwise vortices that grow with downstream distance as they entrain the inviscid core flow, and interact with the inlet shock train generating complex 3D corner SBLI. Interestingly, McDaniel & Edwards [13] reported that the boundary layer separation that ultimately resulted in inlet unstart originated from the inlet corners and sidewalls (see Figure 2 for a schematic of the separation regions). Wagner et al. [6] corroborated these results, although they were

unable to take measurements in the corner. Finally, McDaniel & Edwards postulated that dynamic interactions between the "primary" 2D separation along the inlet walls and the "secondary" separated corner flows may influence the exponential growth of the separated flow that eventually blocks the core flow. These findings were substantiated later by Do et al. [9]. Summarily, it appears that corner separated flows and their interactions with the primary separation play a direct role in the initiation of an unstart event.

Despite the common appearance of corner SBLI in internal and external supersonic flows, comparatively few works have investigated them. Recently, experimental works by Babinsky's group [20, 21, 22, 23] have studied the mean streakline features and wall pressure profiles of 3D corner SBLI generated by impinging shocks in transonic and supersonic flows, as well as the effect of the corner separation extent on the primary separation. Interestingly, they showed that an increased corner separation extent acts to shrink the primary separation for a given inflow condition and shock strength. While data on the mean inlet flow structures and the interactions between them are quite important, they are again limited in their application to the unstart issue, as the phenomenon is continuously transient.

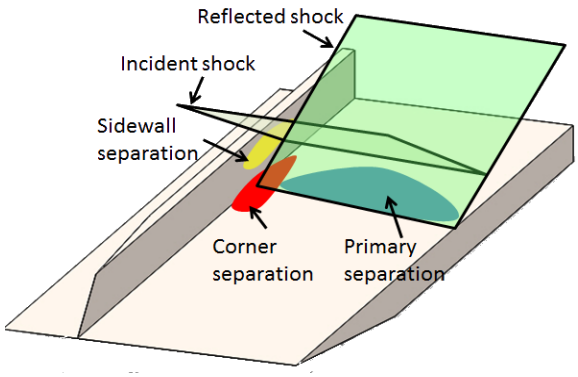

Figure 2. Separation regions during rectangular inlet unstart

Computationally, the extremely fine mesh resolutions necessary to capture the full range of turbulent length scales present in the corner SBLI at Reynolds numbers representative of unstart have limited these investigations to RANS calculations. RANS models have difficulty in capturing the near wall characteristics of corner boundary layers, as well as the aforementioned unsteady aspects of corner SBLI which are of considerable importance in understanding the fundamental physics behind unstart initiation. However, owing to the ever-increasing computational capability of the modern supercomputer, recent direct numerical simulations (DNS) by Poggie et al. [24] have reinforced the importance of SBLI in mixed compression inlets, where they act as broadband amplifiers which can significantly intensify perturbations in the incoming boundary layer. Bisek [25] also performed DNS analysis of the mean and unsteady features of primary and corner SBLI generated by a rectangular channel flow into a compression ramp at $Re_\theta \approx 3{,}000$, although it should be noted that this Reynolds number is still considerably lower than those seen during unstart.

Seemingly then, there is still a great deal to be learned with regards to the unstart-specific SBLI that occur prior to initiation. In our earlier effort [26], we investigated the separated primary and corner boundary layers at mild back pressure to capture the interactions that occur at the early stages of back pressure rise. It was shown that the corner SBLI had several new and distinct features and dominant flow structures that were unique to it. It was further shown that the overall mean and spectral features of the corner and primary separated flows suggested that these flow units had very limited direct interaction. This work aims to gain critical insights into the mean and unsteady features of both primary and corner SBLI units and their mutual interactions with increasing back pressure. The unsteady signatures of both SBLI are characterized, and correlations between pressure fluctuations at various flowfield positions are analyzed.

V.B. Experimental Setup

The experimental setup described at length below is similar to the arrangement of a previous work of the present authors [27]. Several key improvements have been made here, namely higher resolution wall static pressure measurements to more accurately map the pressure profiles of the primary and corner separated flows, and the inclusion of superior signal conditioning to better characterize the unsteady features measured there.

Wind tunnel facility

All experiments were conducted using the North Carolina State University supersonic wind tunnel facility. The tunnel is of the blowdown variety and has a variable throat geometry capable of producing test section Mach numbers ranging from 1.5 to 4.0. For the present work, the Mach number was fixed at 2.5. The test section is of

constant area and measures $150\ mm \times 150\ mm$ in cross section with a length of $650\ mm$. The test section is optically accessible via fused silica windows that are flush with the sidewalls. A removable steel plug in the tunnel ceiling enables top-mounting of the SBLI generator model.

SBLI model

Figure 3 shows a schematic of the SBLI model and a representation of the flow features as they occur. There is a notable resemblance to the upstream portion of a mixed compression inlet. A steel floor plate $370\ mm$ long was placed incident with the tunnel freestream along with two side fences $25\ mm$ tall to form a rectangular channel with a width of $70\ mm$ and a height of $25\ mm$. Note that the leading edges of the floor plate and fences were tapered to a sharp point from the outside edge so as to avoid the formation of unintended compression waves inside the measurement domain. The floor plate was attached to plug mounts that lowered it out of the tunnel ceiling boundary layer and into the uniform freestream. A boundary layer developed over the floor plate and underwent natural transition to turbulence. At each junction of the floor plate and fences, 3D corner boundary layers were formed and both types interacted with the downstream oblique shock wave, generated by a removable compression ramp of adjustable angle and height. The leading edge of the compression ramp was located $300\ mm$ downstream

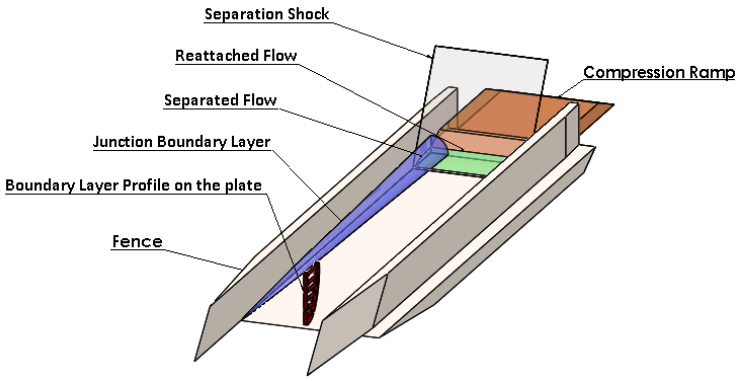

Figure 3. SBLI model and flow feature development

of the floor plate leading edge. At this streamwise position, the incoming boundary layer along the channel floor has a thickness of $\delta = 10\ mm$ at the interaction location for the freestream test Mach number of $M_\infty = 2.5$, as discerned by pitot sweeps in the wall normal direction with the compression ramp and sidewalls removed. The development of the SBLI was tested across a range of shock strengths generated by ramp angles of 12°, 16°, 20°, and 24° (see Table 1 for the corresponding inviscid pressure ratios and a tabulation of incoming flow parameters). The choice in ramp angles follows from previous studies in rectangular isolators, which have shown that unstart initiation typically occurs at around 70% of the normal shock pressure ratio (≈ 7.13 for $M_\infty = 2.5$). From Table 1, it can be observed that the pressure ratio across the range of oblique shock strengths falls between $\approx 30 - 55\%$ of this value, and is believed to be an accurate representation of the increasing adverse pressure gradient that occurs prior to unstart initiation.

Table 1. Incoming flow characteristics

Parameter	Value	
M_∞	2.5	
u_∞	583	m/s
T_∞	140	K
$p_b/p_\infty(12°)$	2.09	(inviscid)
$p_b/p_\infty(16°)$	2.60	(inviscid)

$p_b/p_\infty(20°)$	3.21	(inviscid)
$p_b/p_\infty(24°)$	3.94	(inviscid)
Re_x	5.3×10^7	m^{-1}
Re_θ	39,000	
$\delta_{99\%}$	7	mm
θ	0.77	mm
δ^*	1.20	mm

Flow measurement techniques

Surface streakline flow visualization

Surface streakline flow visualization was performed on the channel floor and sidewalls in order to gain a qualitative understanding of the mean flow structures of the primary and corner SBLI and to aid in the placement of transducers for static wall pressure measurements. The visualization medium was an aluminum oxide and kerosene mixture. The floor plate and sidewalls were painted using flat black latex enamel spray paint from Krylon Inc. to allow for the best possible contrast between the surface and the flow features. Images were recorded after the runs, assuming that the mixture had dried before tunnel shut down. This method provided a time averaged image of the effect of the shear forces of the viscous flow on the oil mixture spread on the surface of the SBLI model. Interpretation of the streakline patterns allows for the identification of the primary and corner separation lines, any vortex patterns, and the approximate extent of the corner boundary layer.

Wall pressure measurements

High-frequency wall pressure measurements were performed in order to obtain the quantitative mean pressure profiles and capture the unsteady characteristics of the primary and corner SBLI. Measurements were made using a high frequency response transducer (Kulite Semiconductor Products, Inc., model XCQ062-15A). The transducer has a nominal diameter of 1.7 mm and a sensing membrane diameter of 0.71 mm. The natural frequency of the transducer diaphragm is 200 kHz, although the effective frequency response is limited to 50 kHz by a protective screen. The signals from the pressure transducers were filtered at 25 kHz using a Stanford Research Systems SR600, and were subsequently digitized at a rate of 100 kHz with a 16-bit Analog-to-Digital converter (National Instruments 9215).

Figure 4 shows the arrangement of the transducers used in this study relative to the observed surface streakline features of interest for one configuration, the minutiae of which are discussed later. Transducers were placed at identical streamwise locations in the corner ($z = 31.8\ mm$) and primary ($z = 0\ mm$) SBLI. Up to eleven transducers were placed in ports in the floor plate such that the center of the transducer closest to the compression corner (depicted here as a yellow rectangle) was at an upstream distance of 1.4 mm, with subsequent transducers every 4.5 mm upstream. The flow direction is from right to left. While the most upstream transducer is located within the incoming boundary layer, the most downstream transducer is located well inside the separated flow.

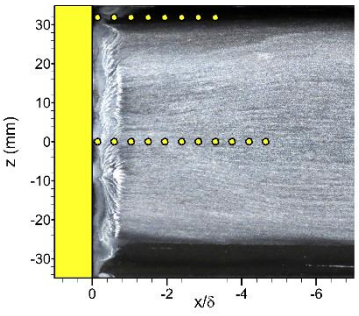

Figure 4. Transducer positions relative to flow features of interest

V.C. Results and Discussion

In the subsequent sections, our findings on the evolution of the SBLI with increasing back pressure are presented. In order to provide context for the results, we include some of the important findings on SBLI with mild back pressures that are discussed in significant detail in an earlier effort [26].

Flow visualization

Figure 5 shows flow visualizations for the four compression ramp angles at $M_\infty = 2.5$. In Fig. 5 the flow direction is from right to left. The x-axis represents the streamwise distance normalized by the boundary layer thickness at the origin. The z-axis represents the spanwise distance. The origin lies along the centerline at the edge of the compression ramp (depicted here as a yellow rectangle). The junction between the floor plate and fence in the positive spanwise direction ($z > 0\ mm$) is referred to as the top corner, while the similar junction in the negative spanwise direction is referred to as the bottom corner.

In Fig. 5(a), the junction boundary layers are shown as dark bands along the top and bottom of the figure. A fairly symmetric growth of the corner boundary layer emanating from the two sides is observed. While the surface streakline visualization does not provide an exact measure of the corner boundary layer thickness, the visualization does provide a lower bound estimate. With this caveat, the spanwise extent of the corner boundary layer is approximately $10\ mm$ at the location just upstream of the shock-induced separation. This thickness is of the same order of magnitude as the centerline turbulent boundary layer discussed previously.

The SBLI separation boundary is visualized in Fig. 5 through pigment accumulation, which occurs in the locations of low shear. In Fig. 5(a), which corresponds to the 12° ramp angle and mildest adverse pressure gradient, three distinct regions of pigment accumulation can be observed – one extending over the bulk of the center region ($-26\ mm < z < 26\ mm$) and the other two distinctly present in the top and bottom corner regions; these represent the primary and corner separations, respectively. The boundary of the primary separation appears fairly two-dimensional over the majority of the span. The primary separation is located at $x/\delta \approx -1$; this location is consistent with the empirical correlations of separation distance of 2D SBLI [28]. This level of consistency and the fairly uniform primary separation boundary suggest that the corner separations do not appear to influence the global extent of the primary separation at this shock strength.

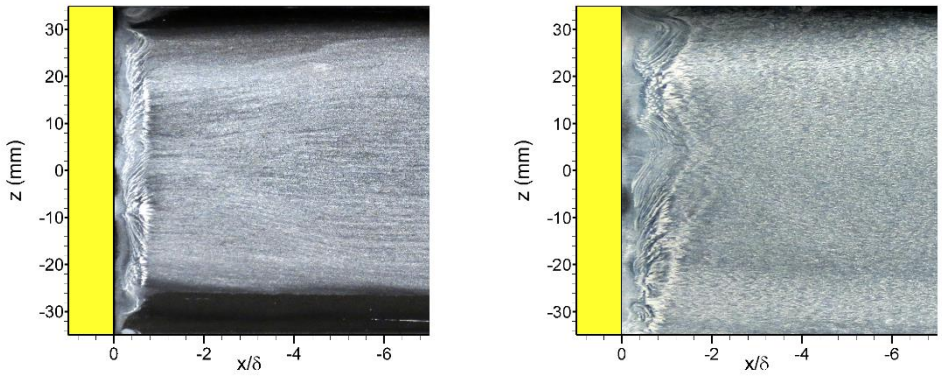

(a) (b)

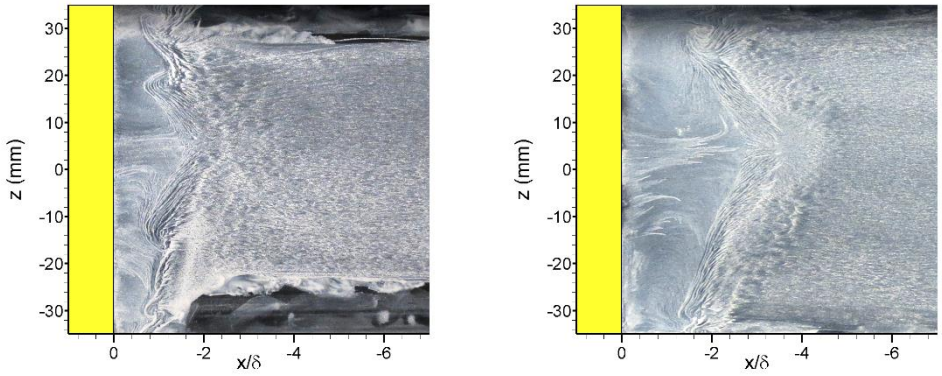

(c) (d)

Figure 5. Full span top view flow visualizations for various configurations at $M_\infty = 2.5$ (a) 12° (b) 16° (c) 20° (d) 24°

In stark contrast to the primary separation, the corner separation regions present in Fig. 5(a) ($z > 30\ mm, z < -30\ mm$) exhibit a highly curved pattern that is indicative of a 3D SBLI. An oval pattern that resembles a corner vortex footprint is discernable on the floor plate between $z \approx 31 - 34\ mm$ and $x \approx -3$ to $-8\ mm$; similar corner vortices have been observed in the recent experimental and computational works described previously [20, 21, 25]. Finally, it can be observed in the top corner of Fig. 5(a) that the corner separation location occurs increasingly upstream as one approaches the floor-sidewall junction. The reason for the observed upstream separation boundary displacement is a decrease in the incoming boundary layer momentum and Mach number as the sidewall is approached.

As the back pressure is increased in Fig. 5(b) - Fig. 5(d), the corner and primary SBLI units exhibit several interesting changes from (and commonalities with) the mildest back pressure case. In the primary SBLI, there is a notable increase in the three-dimensionality of the primary separation line as ramp angle increases, and the primary separation exhibits footprints of tornado-vortices present for all ramp angles above 12°. Interestingly, the primary separation line is pulled out toward the centerline in a curved pattern and the primary separation becomes more curved with increasing back pressure. The extents of the primary and corner separations both increase significantly with back pressure, owing to the increasing magnitude of the adverse pressure gradient. While the corner separation line is displaced upstream with increasing ramp angle, the extent of corner vortex remains relatively constant over the range of back pressures employed. This observation is also corroborated with the vortex length determined using r.m.s. wall pressure profiles discussed subsequently, and suggests that the primary separation does not appear to influence the corner vortex features.

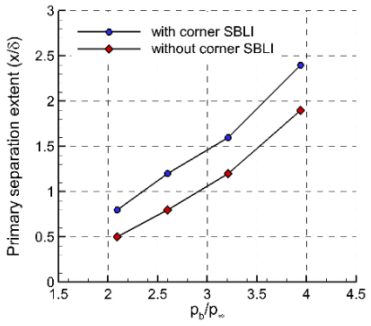

Figure 6. Spanwise mean separation extent with and without corner SBLI for various back pressures at $M_\infty = 2.5$

To determine any modification of the primary separation by the corner SBLI, a comparison is drawn between approximate spanwise-averaged primary separation locations with and without the presence of

the corner SBLI at different back pressures. To obtain the separation extent without corner SBLI, the long fences that bound the compression ramp were replaced by short fences that extended 1δ into the incoming boundary layer. Figure 6 shows the spanwise-mean primary separation location with and without corner SBLI at different back pressures. It can be observed that there is a significant upstream displacement of the separation location at all back pressures employed. Further, it can be observed that this effect is exaggerated as the back pressure is increased. For example, whereas the primary separation line is displaced by 0.3δ upstream for 12° ramp angle, the corresponding value is 0.5δ for the 24° ramp angle. This displacement magnitude is further exaggerated if one considers the primary separation location just along the centerline, while maintaining the overall qualitative trend discussed above. Thus, it is quite clear that the corner boundary layer acts to significantly enlarge the primary separation with increasing back pressure in addition to inducing significant three-dimensionality in the primary separation.

Proposed physical model

A physical model was developed to explain some of the mean flow interactions that result in the observed additional enlargement of the mean primary separation with the corner SBLI, and the transition of the primary separation from a 2D to 3D SBLI with increasing ramp angle. To explain the mean enlargement, first note that the presence of the corner boundary layer imposes a blockage on the incoming flow. As shown in Figure 7, this blockage introduces a transverse pressure gradient directed from the corner towards the centerline resulting in vena-contracta. The transverse pressure gradient could also push the low-momentum fluid from the corner boundary layer into the primary boundary layer, resulting in a momentum decrease there. This momentum decrease would cause the primary boundary layer to separate with larger propensity and, hence, an overall increase in separated flow extent. Further, the momentum decrease would be largest at the centerline where the low momentum fluid from both corners accumulates; this could cause the characteristic upstream bulge in the separation line at the centerline.

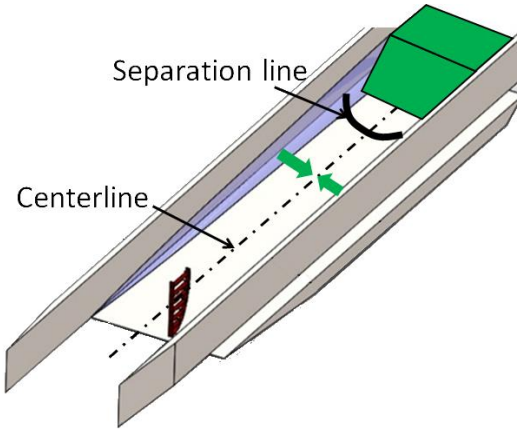

Figure 7. Illustration of mechanisms causing 3D SBLI *(green arrows show the direction of pressure gradient and the direction of decrease in incoming boundary layer momentum)*

An important question to answer is whether the upstream displacement of the primary separation location is in fact a simple vena-contracta effect or if the primary separation enlargement has contributions from the modifications of the incoming boundary layer due to the migration of low momentum fluid. To answer this question, boundary layer profile measurements were performed with and without sidewall fences to examine changes induced by the corner blockage. Figure 8 shows the boundary layer profile measured along the centerline with and without the corner blockage. It can be observed that the corner blockage introduces a large velocity deficit into the centerline boundary layer. This velocity deficit is expected due to the accumulation of low momentum fluid from both sides. To further test this hypothesis, the boundary layer profile is also shown at the quarter span location with and without the presence of corner blockage. At the quarter span location, a smaller accumulation of the low momentum fluid is expected. It can be observed that the velocity deficit is considerably smaller at the quarter span location when compared to the centerline, a result consistent with this expectation. Very importantly the freestream velocity with and without blockage has the same value; it should also be noted that freestream is located well within the height of the side fences. Thus, we conclude that the upstream displacement of the primary separation location with increasing back pressure is largely due to the modifications imposed on the incoming boundary layer by the corner blockage.

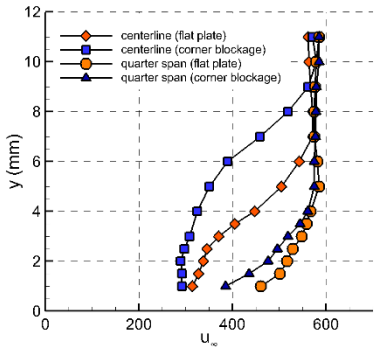

Figure 8. Boundary layer profiles at centerline and quarter span with and without corner blockage effect

Wall pressure measurements

Mean wall pressures

Figure 9 displays the evolution of the mean wall pressures at each transducer position normalized by the static pressure in the incoming turbulent boundary layer across the range of compression strengths, averaged over three independent experimental runs each. Error bars were added to indicate the two-sided 95 percent confidence interval. In Fig. 9(a), the pressure along the centerline increases gradually as the compression ramp leading edge is approached, from the freestream value at $x/\delta \approx -1$ to a peak of $\bar{p}_w/p_\infty = 1.55$ at the most downsteam location of $x/\delta \approx -0.15$. The location of the initial pressure rise and the peak wall pressure nearest the compression ramp are consistent with values reported in 2D SBLI at similar Mach numbers [28, 29]. The pressure contour in the corner SBLI depicted in Fig. 9(a) is highly similar to that of the centerline, although it should be noted that for a given streamwise position the pressure rise in the corner is lower by as much as $\bar{p}_w/p_\infty = 0.16$ (11%). This "smearing" of the corner adverse pressure gradient has been exhibited in corner SBLI generated by impinging normal shocks [20].

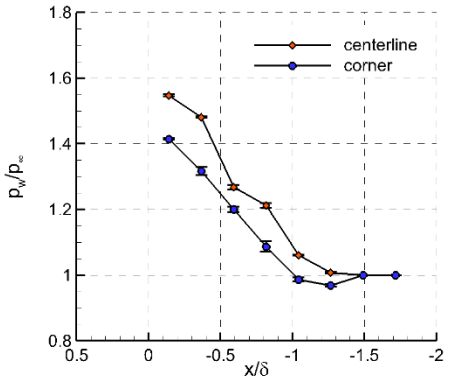

(a)

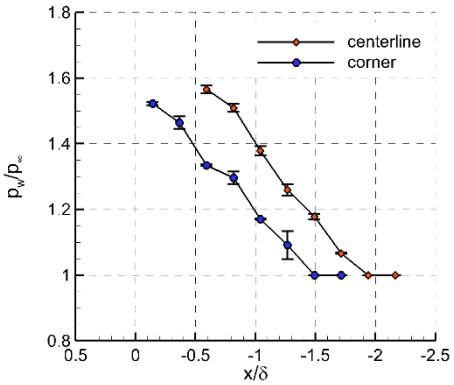

(b)

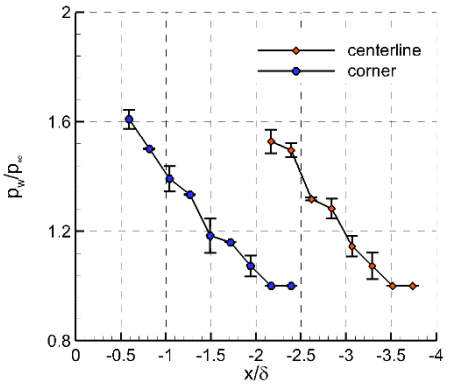

(c)

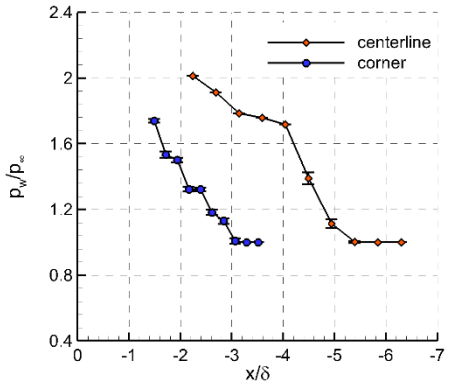

(d)

Figure 9. Mean wall pressures for various configurations at $M_\infty = 2.5$ (a) 12° (b) 16° (c) 20° (d) 24°

As the back pressure is increased, flow visualizations in Fig. 5 revealed that the separation shock is pulled out at the centerline while the corner separation lags behind at a distance downstream. This is also revealed in the mean pressure profiles of Fig. 9(b) – Fig. 9(d), which show that the pressure first begins to increase at a progressively upstream location in the primary SBLI compared to corner SBLI. Further, as the extent of the primary separated flow increases with back pressure, the pressure gradient along the primary separation is considerably reduced. For example, whereas the wall pressure increases by 60% over 1δ for the 12° case, the pressure increases by 100% over 3δ for the 24° case. Interestingly, we can observe two distinct regions of pressure gradients in Fig. 9(d) – a larger pressure gradient region between $-4 \geq x/\delta \geq -5.2$ that corresponds to the intermittent region of the SBLI and a smaller pressure gradient region between $-2 \geq x/\delta \geq -4$, which corresponds to the separated flow region. Further, Fig. 9(a) – 9(d) show that the intermittent region exhibits similar pressure gradient values for all back pressures considered. Similar observations on the dichotomy of pressure gradient along the SBLI and the similarity of the gradients in the intermittent region over different shock strengths are also made by Dolling & Or [14] in 2D SBLIs.

Root-mean square pressures

The streamwise evolutions of the wall pressure fluctuations in the primary and corner SBLI with increasing adverse pressure gradient are shown in Figure 10. Note that the r.m.s. pressure at each transducer is normalized by its respective mean shown in Fig. 9, to enable direct comparison between various streamwise positions and compression strengths.

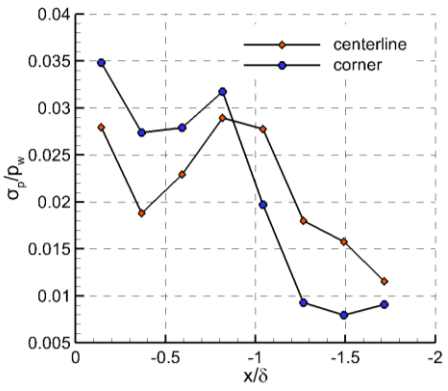

(a)

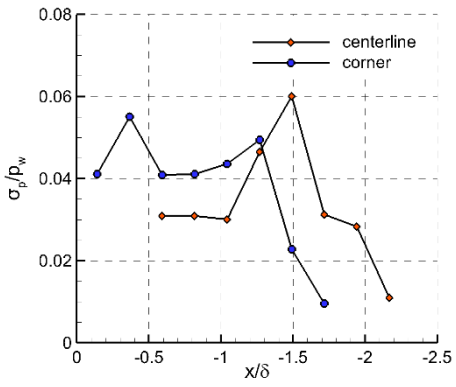

(b)

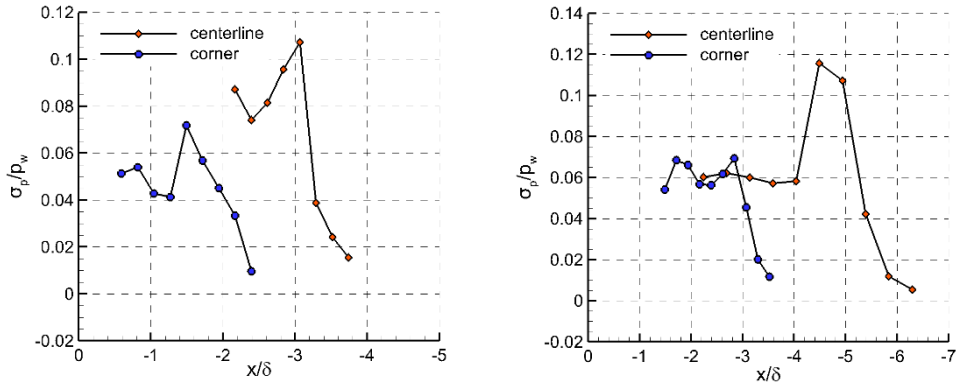

(c) (d)

Figure 10. R.M.S. pressures for various configurations at $M_\infty = 2.5$ (a) 12° (b) 16° (c) 20° (d) 24°

The results of the 12° configuration shown in Fig. 10(a) provide a unique opportunity to directly compare tendencies of the unsteady pressures of the primary and corner SBLI at the same streamwise positions, and will serve as a worthy introduction of trends that evolve with the back pressure ratio. The centerline exhibits a rise from $\sigma_p/\bar{p}_w = 0.012$ in the incoming boundary layer to a distinct peak of $\sigma_p/\bar{p}_w = 0.029$ at $x/\delta = -0.8$. The peak in unsteady pressure here is indicative of the intermittent region location, and is caused by the frequent passage of the separation shock foot. There is a drop in pressure fluctuation in the downstream separated flow, followed by an increase as the compression corner is approached. These trends in pressure fluctuation are consistent with the accumulated r.m.s. pressure profiles of 2D SBLI found in literature [14].When observing the corner r.m.s. pressure trends, there is a slight decrease in the pressure fluctuation magnitude of the incoming corner boundary layer compared to that of the centerline. This is probably due to increased viscous dissipation caused by the additional sidewall boundary layer. Another possibility is that the turbulent streaks that are responsible for the pressure fluctuations are located further away from the wall in the corner boundary layer compared to the primary boundary layer. At this point, we cannot definitively ascertain the cause for this smaller σ_p. Downstream of the incoming boundary layer, the trends exhibited are largely similar to those of the centerline, with a peak in $\sigma_p/\bar{p}_w$ at $x/\delta = -0.8$, a streamwise position coincident with both the primary intermittent region and the upstream periphery of the corner vortex shown in Fig. 5(a), followed by a decreased in $\sigma_p/\bar{p}_w$ within the corner vortex and a subsequent increase in $\sigma_p/\bar{p}_w$ at the most downstream measurement location. Interestingly, the increase in $\sigma_p/\bar{p}_w$ at the most downstream location occurs in close proximity to the downstream edge of the corner vortex. These two peaks are a consistent feature of all the corner r.m.s. pressure curves depicted in Fig. 10, and we observe that they do in fact occur at the upstream and downstream peripheries of the corner vortex at all back pressures. Similar instances of these peaks have been reported in the fin-SBLI studies of Alvi & Settles [30], also in the recent DNS of Bisek [25].

Considering the profiles of $\sigma_p/\bar{p}_w$ as the back pressure is increased in Fig. 10(b) – Fig. 10(d), it can be observed that the trends exhibited are similar to those of the 12° case. While both the primary and corner intermittent regions (identified by the most upstream peak in $\sigma_p/\bar{p}_w$) move upstream with ramp angle, the centerline separation line is displaced upstream to a greater extent as evidenced by a consistently increasing separation between the corner and primary SBLI intermittent region with increasing back pressure - a result which is consistent with the earlier flow visualization.

The r.m.s. pressure curves depicted in Fig. 10 enable the determination of length scales that will later prove to be necessary in the calculation and comparison of normalized frequency spectra. In 2D SBLI, a typical characteristic length is the separation length L_{sep}, defined as the streamwise distance from the compression ramp leading edge to

the intermittent region. As previously noted, the two distinct peaks in pressure fluctuation present in the corner lend themselves to the definition of a separate vortex length scale L_v, which is the streamwise distance between the upstream and downstream peaks that are observed to coincide with the corner vortex edges. Table 2 shows the values of L_{sep} and L_v for each configuration that were calculated from Fig. 10; note that L_{sep} corresponds to the *primary* separation distance measured using centerline $\sigma_p/\bar{p}_w$ data to identify the intermittent region.

Table 2. Separation and vortex length scales for various configurations at $M_\infty = 2.5$

Ramp angle	$L_{sep}(mm)$	$L_v\ (mm)$
12°	8.1	8.1
16°	15.0	8.9
20°	30.6	6.7
24°	44.6	11.2

From Table 2, the increase in primary separation extent with ramp angle is readily evident. Interestingly, no such pattern is evident in the corner vortex length, with the size remaining relatively constant. This supports the earlier trend observed in Fig. 5, and suggests that while the primary separation extent is modified by increasing shock strength, the corner vortex size may respond to different influencing mechanisms.

Wall static pressure power spectrum

Power spectral densities of the corner and primary SBLI intermittent regions were computed in order to gain insights into the characteristic separated flow motions that create the unsteady mechanical loading. Figure 11 shows the frequency-multiplied power spectrum of the primary and corner SBLI intermittent regions for each ramp angle. The separation length scales from Table 2 were used in the determination of the Strouhal number ($St_{L_{sep}}$), which is also displayed. For the 12° case in Fig. 11(a), the primary SBLI exhibits a range of dominant frequencies from $f \approx 100\ Hz$ to $3\ kHz$ ($St_{L_{sep}} \approx 0.001 - 0.05$). This Strouhal number range is very consistent with the previously reported values of 2D SBLIs, as noted in our earlier work [26]. Note the slight upturn at the high-end of the frequency range, caused by shock oscillation due to passage of turbulent structures. Interestingly, the spectral energy content of the corner SBLI is considerably more focused than the primary SBLI, with a spectral peak at $\approx 3.5\ kHz$ ($St_{L_{sep}} \approx 0.05$). This peak suggests that the transient mechanical loading in the corner SBLI is less aperiodic than that of the primary SBLI.

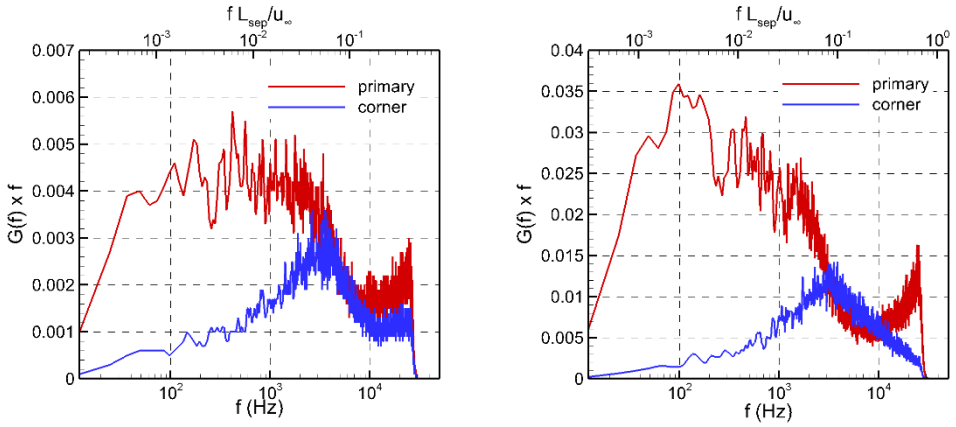

(a) (b)

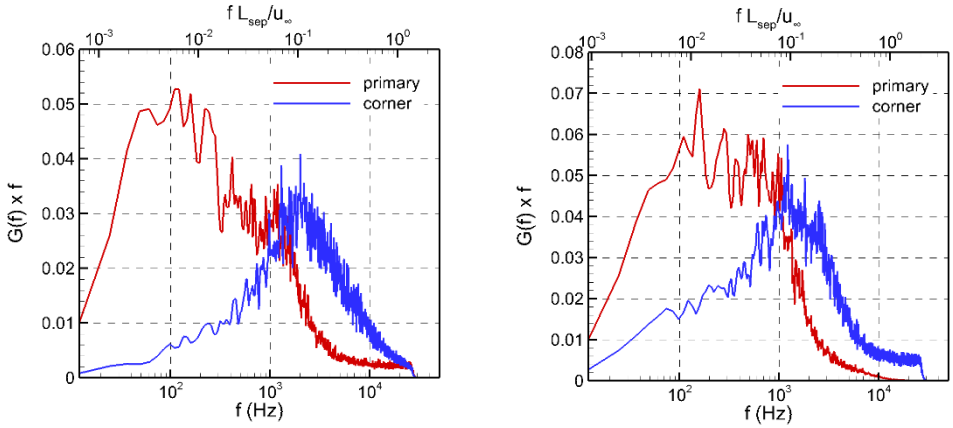

(c) (d)

Figure 11. Comparison of pressure power spectra of intermittent regions for various configurations at $M_\infty = 2.5$ (a) 12° (b) 16° (c) 20° (d) 24°

As the compression ramp angle is increased, both the primary and corner SBLI exhibit spectral shifts toward lower frequencies. For ease of observation, the peak frequencies and Strouhal numbers of each SBLI are tabulated in Table 3. Note that the range of peak Strouhal numbers exhibited for the primary SBLI are in line with previous compilations of canonical 2D SBLI. From Table 3, the shift toward low frequency is evident in the corner as the peak frequency consistently decreases with increasing ramp angle. This is not discernable from the centerline data in Table 3 due to the broadband nature of the primary SBLI, and is more easily viewed by comparing Fig. 11(a) with Fig. 11(d), as the dominant frequency range decreases from $f \approx 100\ Hz$ to $3\ kHz$ at 12° to $f \approx 100\ Hz$ to $1200\ kHz$ at 24°. Interestingly, the dominant corner frequency seems to consistently occur very near where the primary SBLI begins to exhibit spectral decay at higher frequencies, although it remains to be seen whether this result is meaningful or coincidental.

Table 3. Peak frequencies and Strouhal numbers for various configurations at $M_\infty = 2.5$

Ramp angle	Primary		Corner		
	$f\ (Hz)$	$St_{L_{sep}}$	$f\ (Hz)$	$St_{L_{sep}}$	St_{L_v}
12°	410	0.0057	3490	0.049	0.049
16°	100	0.0026	3140	0.081	0.048
20°	120	0.0063	1920	0.100	0.022
24°	160	0.0122	1200	0.091	0.023

While the separation scale of the primary SBLI is known, a great deal of uncertainty still remains regarding the choice of an appropriate characteristic length for scaling of the corner SBLI characteristic unsteadiness. In our earlier work with mild back pressure [26], it was shown that both L_{sep} and L_v provided similar values of peak Strouhal number that are consistent with fin-SBLI literature. Of the two, L_v was more physically meaningful, as the corner vortex appeared to drive the unsteady separation at low back pressures. Now the question becomes how the peak Strouhal numbers based on L_{sep} and L_v evolve with increasing back pressure; in other words whether or not the corner vortex motions will continue to dominate/drive the characteristic motions of the corner SBLI. To answer this question, the peak Strouhal numbers for different back pressures defined using L_{sep} and L_v are shown in Table 3. It can be observed that St_{L_v} seems to have closer agreement in values for low back pressures (12° and 16° ramp

angles), while higher back pressures exhibit large scatter in St_{L_v} values. Similarly, while the $St_{L_{sep}}$ values for 12° and 16° show considerable difference, $St_{L_{sep}}$ appears to collapse more evenly at higher shock strengths $(16°, 20°, 24°)$. Figure 12 shows this disparity through the nondimensional frequency spectra of the primary and corner intermittent regions at each back pressure for L_{sep} and L_v (note that each spectrum is normalized by the area beneath it for ease of comparison). From Fig. 12(a), it is evident that L_{sep} remains the appropriate characteristic length for scaling of the primary SBLI unsteadiness. In contrast, Fig. 12(b) and Fig. 12(c) show the corner spectra based on the separation and vortex length scales, respectively, and reveal the aforementioned scatter between higher and lower back pressures discussed previously. The results of Fig. 12 and Table 3 suggest that at mild back pressures, L_v appears to scale the characteristic unsteadiness of corner SBLI while L_{sep} scales the corner SBLI unsteadiness more neatly at high back pressures. This suggests that the corner SBLI transitions from being a distinct, local unit driven by corner vortex pulsations at low back pressures (consistent with the author's previous work [26]) to an interacting portion of a global separation unit that is influenced by global driving mechanisms.

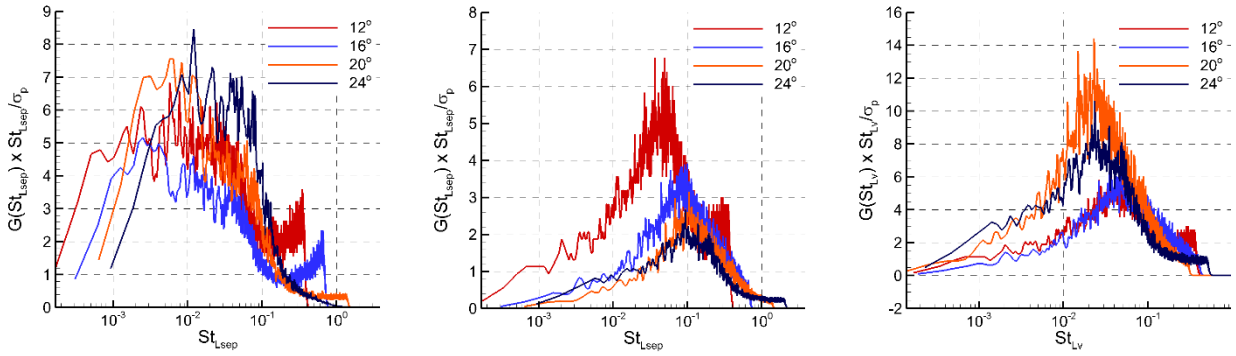

(a) (b) (c)

Figure 12. Power spectra of primary and corner SBLI intermittent regions using L_{sep} and L_v (a) primary SBLI using L_{sep} (b) corner SBLI using L_{sep} (c) corner SBLI using L_v

Cross-coherence and mechanisms driving unsteadiness

The sources that drive the primary and corner SBLI at different back pressures were studied further to elucidate how the driving mechanisms evolve with adverse pressure gradient. Two-point cross-coherence studies were performed at each imposed back pressure to determine the response of the separation shock motion to pressure fluctuations originating from the incoming boundary layer and the downstream separated flows. Cross-coherences were performed individually between the intermittent region and upstream transducer pressure signals, and intermittent region and downstream transducer pressure signals, each separated by $x/\delta \approx 0.4$ from the intermittent region. The degree of coupling between two signals at a given frequency relates directly to the cross-coherence between them at that frequency, with a magnitude of zero indicating an uncoupled system and a magnitude of unity indicating a linear coupling.

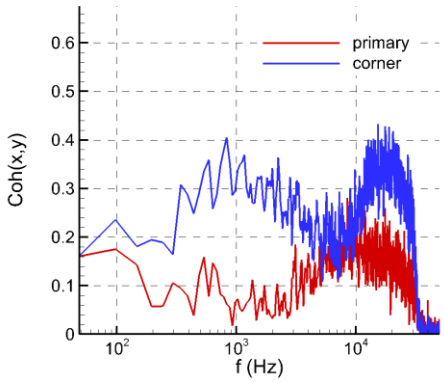

(a)

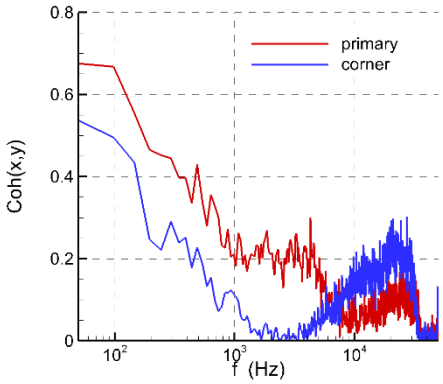

(b)

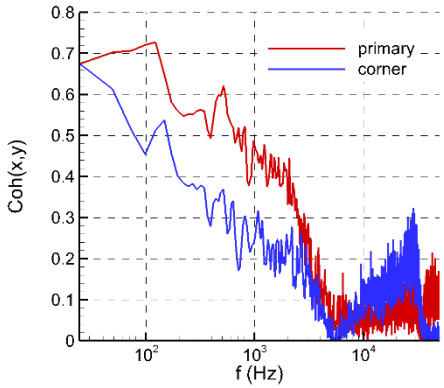

(c)

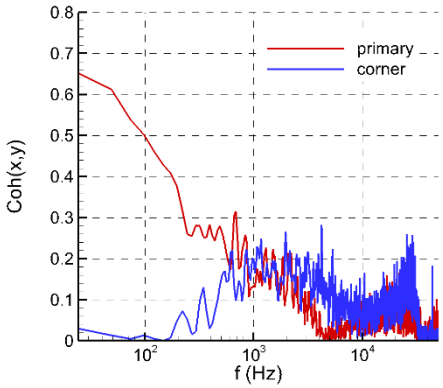

(d)

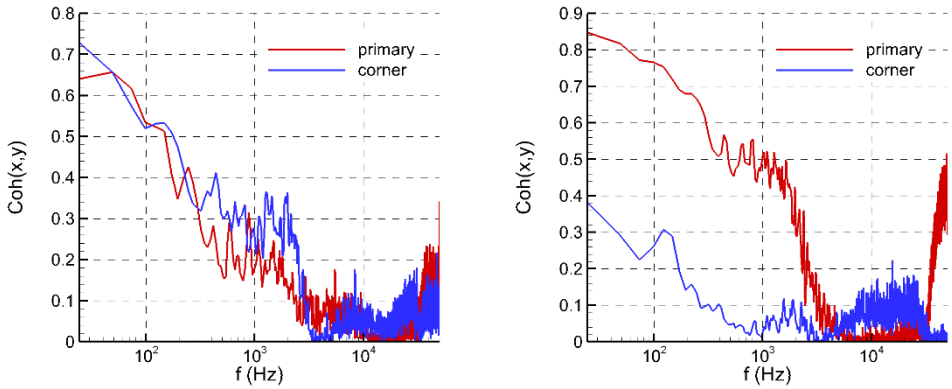

(e)

(f)

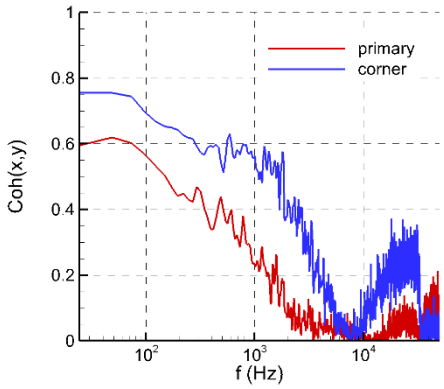

(g)

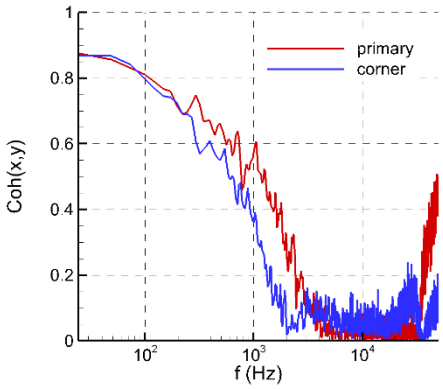

(h)

Figure 13. Cross-coherence spectrum of intermittent regions with upstream boundary layer and downstream separation for various configurations at $M_\infty = 2.5$ (a) 12° upstream (b) 12° downstream (c) 16° upstream (d) 16° downstream (e) 20° upstream (f) 20° downstream (g) 24° upstream (h) 24° downstream

Figure 13 depicts the cross-coherence spectra of the primary and corner SBLI with the upstream and downstream pressure signals for the range of configurations tested. Fig. 13(a) displays the cross-coherence spectrum of the primary and corner intermittent regions with the incoming boundary layer for the 12° ramp angle. Note that while the magnitude of cross-coherence may be considerable at a given frequency, it is only significant if this frequency falls within the dominant frequency ranges shown in Fig. 11. With this background, it is evident that for the 12° case shock motion of the primary SBLI exhibits a cross-coherence magnitude of ≈ 0.1 across its unsteady frequency range of $100\ Hz - 3\ kHz$, indicating little coupling with the turbulent fluctuations there. This trend is consistent with the DNS work of Priebe and Martín, who performed similar cross-coherence studies in a

compression ramp SBLI at Mach 2.9 [31]. By comparison, the corner separation is much more coupled at its dominant frequency of 3.5 kHz. When considering the cross-coherence spectrum of the intermittent regions with the downstream separation in Fig. 13(b) the opposite trend is evident; the primary SBLI shock motion is significantly more coupled with the downstream separation at $\approx 0.2 - 0.3$ across its frequency range. By contrast, the corner shows coupling less than ≈ 0.1 with the downstream separation. The differences in mechanisms to which the primary and corner SBLI respond at this low shock strength support the hypothesized independence of the two units at mild back pressures.

As the adverse pressure gradient is increased, the trends evident in the cross-coherence spectra of the primary SBLI remain largely the same in the downstream separation region, as the separation shock motion consistently couples more with the downstream separation. Interestingly, there is also an increasing coupling of the primary separation shock with incoming boundary layer fluctuations with increasing back pressure. Similarly, the corner separation shock begins to couple appreciably with the motions of the downstream corner vortex as well as incoming boundary layer fluctuations as ramp angle increases, such that at $24°$ it responds nearly equally to the vortex motions and incoming turbulent fluctuations. In Fig. 13(g) and Fig. 13(h), the primary and corner cross-coherence spectra begin to resemble one another, suggesting that the two will respond similarly to perturbation acting almost like a single unit. This observation further strengthens the hypothesis that the corner and primary SBLI have coupled into a coherent unit that responds similarly to the upstream and downstream fluctuations. An important caveat is that both the primary and corner SBLI units are highly 3D even in mean. Thus, the similarity in coupling of separation shock motion to one downstream location may not be enough to establish that the corner and primary SBLI respond in a like manner to all downstream fluctuations. Similarly, the wall pressure fluctuations in the incoming boundary layer may not capture the global changes in the incoming momentum of non-canonical boundary layers that occur along the corner. Thus, similarity in the shock response to upstream fluctuations should also be treated with caution. In a future effort, we will address these issues through coupled flow imaging and wall pressure quantification.

Importance to Inlet Unstart

What do the preceding observations mean for unstart physics? First, the stark difference in the spectral signatures and driving sources implies that the corner SBLI and primary SBLI pulsate as distinct units at mild back pressures, consistent with our previous work [26]. Thus, the initial interactions that precede inlet unstart occur at a local level at different separated flow locations, which somehow couple with one another to result in global motion; this is in contrast to the existing belief that unstart occurs as a result of global interactions that drive the entire separated flow as a single coherent unit [10]. Second, the fact that a considerable band of overlapping frequencies between corner and primary SBLI exists opens the possibility of *resonant/dispersive interactions* between the two SBLI units, where pressure fluctuations originating from the corner SBLI in the overlapping frequencies are amplified in the primary separation leading to a strong instability and potentially larger instantaneous primary separation. Third, since the corner and primary SBLI have very different features and contributing mechanisms, simulations into the dynamics of the unstart SBLI unit require high-fidelity models that capture both corner and primary separation accurately, and traditional $k - \epsilon$ models that tend to under-predict the corner separation may prove inadequate.

VI. Conclusions

An experimental investigation is made into the primary and corner SBLI generated in a rectangular channel flow by compression ramps of various angles at $M_\infty = 2.5$. Selection of the ramp angles follows inviscid pressure ratios representative of a buildup to unstart initiation in a rectangular mixed compression inlet. Surface streakline flow visualization shows a two-dimensional primary SBLI structure at mild shock strengths, while the presence of a vortex footprint in the corner SBLI indicates a three-dimensional flow structure there. The primary separation extent is modified considerably at the centerline for higher ramp angles, while the corner vortices remain relatively constant in size and move laterally towards the centerline. Mean wall static pressure measurements show an initial smearing of the adverse pressure gradient in the corner, similar to previous findings [22]. An increase in ramp angle brings an increasing streamwise distance between the initial pressure rise of the primary and corner SBLI that is consistent with the modification suggested by the flow visualization. The r.m.s. pressure contours show a single

distinct peak along the centerline at the intermittent region, and two peaks in the corner SBLI that coincide with the peripheries of the corner vortex. Pressure power spectra reveal that the energy content of the corner unsteady motions is considerably more focused than its counterpart in the primary SBLI, and that the appropriate length scale for the calculation of nondimensional frequency in corner SBLI may change as the inviscid pressure ratio is increased and the corner SBLI is integrated into the global SBLI. Finally, cross-coherences show that the primary shock motion couples more with pressure fluctuations in the downstream separation than the incoming boundary layer for a given ramp angle, although the magnitude of cross-coherence increases between the intermittent region and upstream boundary layer with ramp angle. The corner trends are similar but inverted, as the corner shock motions couple more so with the incoming boundary layer but are increasingly responsive to the motion of the corner vortex with increasing back pressure. These results suggest two distinct stages in the unstart-specific SBLI units, one where the initial primary and corner SBLI act as mutually independent entities at mild shock strengths, and a later stage wherein the corner SBLI begins to modify the primary SBLI, although further investigation is needed to determine the driving mechanisms of this transition.

VII. References

[1] S. Farokhi, Aircraft Propulsion. Second ed., West Sussex: John Wiley & Sons, 2014.

[2] D. Riggins, R. Tackett, T. Taylor and A. Auslender, "Thermodynamic analysis of dual mode scramjet engine operation and performance," *AIAA Paper, 8059,* 2006.

[3] E. Curran, W. Heiser and D. Pratt, "Fluid Phenomena in Scramjet Combustion Systems," *Annual Review of Fluid Mechanics,* pp. 323-360, 1996.

[4] T. Mehuron, "Air Force World, Second X-51 Test Cut Short," *Air Force magazine,* vol. 94, pp. 17-18, 2011.

[5] J. L. Wagner, K. B. Yuceil, A. Valdavia, N. T. Clemens and D. S. Dolling, "Experimental Investigation of Unstart in an Inlet/Isolator Model in Mach 5 Flow," *AIAA J,* vol. 47, no. 6, pp. 1528 - 1542, 2009.

[6] J. L. Wagner, K. B. Yuceil and N. T. Clemens, "Velocimetry Measurements of Unstart in an Inlet-Isolator Model in Mach 5 Flow," *AIAA J,* vol. 48, no. 9, pp. 1875 - 1888, 2010.

[7] W. R. Hawkins and E. J. Marquart, "Two-Dimensional Generic Inlet Unstart Detection at Mach 2.5–5.0," *AIAA-95-6016,* 1995.

[8] A. R. Weiting, "Exploratory Study of Transient Unstart Phenomena in a Three-Dimensional Fixed-Geometry Scramjet Engine," *NASA TN D-8156,* 1976.

[9] H. Do, S. Im, M. G. Mungal and M. A. Cappelli, "The influence of boundary layers on supersonic inlet flow unstart induced by mass injection," *Experiments in Fluids,* vol. 51, pp. 679 - 691, 2011.

[10] S. Laurence, S. Karl, J. Schramm and K. Hannemann, "Transient fluid-combustion phenomena in a model scramjet," *Journal of Fluid Mechanics,* vol. 722, pp. 85 - 120, 2013.

[11] S. O'Byrne, M. Doolan, S. R. Olsen and A. F. P. Houwing, "Analysis of Transient Thermal Choking Processes in a Model Scramjet Engine," *Journal of Propulsion and Power,* vol. 16, no. 5, pp. 808 - 814, 2000.

[12] K. S. McDaniel and J. R. Edwards, "Simulation of Thermal Choking in a Model Scramjet Combustor," *AIAA 99-3411,* 1999.

[13] K. S. McDaniel and J. R. Edwards, "Three-Dimensional Simulation of Thermal Choking in a Model Scramjet Combustor," *AIAA 2001-0382,* 2001.

[14] D. Dolling, "Fluctuating Loads in Shock Wave/Turbulent Boundary Layer interaction: Tutorial and Update," in *31st Aerospace Sciences Meeting & Exhibit,* 1993.

[15] D. Knight, H. Yan, P. A.G. and A. Zheltvodov, "Advances in CFD prediction of shock wave turbulent boundary layer interactions," *Progress in Aerospace Sciences,* pp. 121-184, 2003.

[16] A. Zheltovodov, "Shock wave/turbulent boundary layer interactions - fundemental studies and applications," *AIAA paper, ,* 1996.

[17] N. T. Clemens and V. Narayanaswamy, "Low-Frequency Unsteadiness of Shock/Wave Boundary Layer Interactions," *Annual Review of Fluid Mechanics,* pp. 469-492, 2014.

[18] D. V. Gaitonde, "Progress in Shock Wave/Boundary Layer Interactions," in *43rd Fluid Dynamics Conference,*

2013.

[19] M. Smart, "Design of Three-dimensional Hypersonic Inlets with Rectangular to Elliptical Shape Transition," *36th AIAA Aerospace Sciences Meeting and Exhibit*, 1998.

[20] D. Burton and H. B. P. Babinsky, "Experimental Investigation into Parameters Governing Corner Interactions for Transonic Shock Wave/Boundary Layer Interactions," *AIAA Paper*, *871*, 2010.

[21] D. Burton and H. Babinsky, "Corner separation effects for normal shock wave/turbulent boundary layer interactions in rectangular channels," *Journal of Fluid Mechanics*, vol. 707, pp. 287-306, 2012.

[22] P. Bruce, D. Burton and H. Babinsky, "Corner effect and separation in transonic channel flows," *Journal of Fluid Mechanics*, vol. 679, pp. 247-262, 2011.

[23] H. Babinsky and J. Oorebeek, "Corner effects in reflecting oblique shock-wave/boundary layer interactions," in *51st AIAA Aerospace Sciences Meeting* , Dallas/Ft. Worth, 2013.

[24] J. Poggie, N. Bisek, R. Kimmel and S. Stanfield, "Spectral Characteristics of Separation Shock Unsteadiness," *AIAA Journal*, vol. 53, no. 1, pp. 200-214, 2015.

[25] N. Bisek, "Sidewall Interaction of a Supersonic Flow over a Compression Ramp," in *53rd AIAA Aerospace Sciences Conference*, 2015.

[26] M. Funderburk and V. Narayanaswamy, "Experimental Investigation of Primary and Corner Shock Boundary Layer Interactions at MIld Back Pressure Ratios," *Physics of Fluids*, 2016 (accepted for publication).

[27] A. Hegde, M. Funderburk, H. J. and V. Narayanaswamy, "Experimental Investigation into Shock Induced Corner Boundary Layer Separation," *45th Annual AIAA Fluid Dynamics Conference*, 2015.

[28] G. Settles, T. Fitzpatrick and S. Bogdonoff, "Detailed Study of Attached and Separated Compression Corner Flowfields in High Reynolds Number Supersonic Flow," *AIAA journal*, vol. 17, no. 6, pp. 579-585, 1979.

[29] D. Dolling and C. Or, "Unsteadiness of shock wave structure in attached and separated compression ramp flows," *Experiments in Fluids*, vol. 3, pp. 24-32, 1985.

[30] F. Alvi and G. Settles, "Physical Model of the Swept Shock Wave/Boundary-Layer Interaction Flowfield," *AIAA Journal* , vol. 30, no. 9, pp. 2252-2258, 1992.

[31] S. Priebe and M. Martin, "Low-frequency unsteadiness in shock wave-turbulent boundary layer interaction," *Journal of Fluid Mechanics*, vol. 699, pp. 1-49, 2012.

REPORT DOCUMENTATION PAGE

Form Approved
OMB No. 0704-0188

1. REPORT DATE *(DD-MM-YYYY)*	2. REPORT TYPE	3. DATES COVERED *(From - To)*
02-04-2019	Final Performance	30 Sep 2015 to 29 Sep 2018

4. TITLE AND SUBTITLE
Experimental Investigation of Dynamic Flow Interactions in Shock-Induced Separated Corner Boundary Layers

5a. CONTRACT NUMBER

5b. GRANT NUMBER
FA9550-15-1-0296

5c. PROGRAM ELEMENT NUMBER
61102F

6. AUTHOR(S)
Venkateswaran Narayanaswamy

5d. PROJECT NUMBER

5e. TASK NUMBER

5f. WORK UNIT NUMBER

7. PERFORMING ORGANIZATION NAME(S) AND ADDRESS(ES)
NORTH CAROLINA STATE UNIVERSITY
2701 SULLIVAN DR, STE 240, CAMPUS BX 7
RALEIGH, NC 27695-7003 US

8. PERFORMING ORGANIZATION REPORT NUMBER

9. SPONSORING/MONITORING AGENCY NAME(S) AND ADDRESS(ES)
AF Office of Scientific Research
875 N. Randolph St. Room 3112
Arlington, VA 22203

10. SPONSOR/MONITOR'S ACRONYM(S)
AFRL/AFOSR RTA1

11. SPONSOR/MONITOR'S REPORT NUMBER(S)
AFRL-AFOSR-VA-TR-2019-0081

12. DISTRIBUTION/AVAILABILITY STATEMENT
A DISTRIBUTION UNLIMITED: PB Public Release

13. SUPPLEMENTARY NOTES

14. ABSTRACT
Inlet unstart is initiated and sustained by avalanche growth of separated flows resulting from the interaction between different shock boundary layer interaction (SBLI) units within rectangular isolators. In this study, an experimental campaign is undertaken to investigate the primary and corner SBLI dynamics to provide unprecedented insights into the flow interactions that precede and propagate rectangular inlet/isolator unstart. Surface streakline visualization, high-frequency wall pressure measurements, and dynamic streakline visualization were performed to delineate how corner and primary separated flow units mutually interact with one another with an increasing imposed (steady) back pressure, and how this interaction results in the avalanche growth of separated flows. Our results provided unique insights into the dynamics of the primary and corner separated flows and the sources that drive these separation units. Further our results suggest that the corner separation is indeed an integral driving component of the separated flow dynamics of the entire isolator flow.

15. SUBJECT TERMS
corner flow, corner flow AND unstart, corner flow AND shock boundary layer interaction

16. SECURITY CLASSIFICATION OF:			17. LIMITATION OF ABSTRACT	18. NUMBER OF PAGES	19a. NAME OF RESPONSIBLE PERSON
a. REPORT	b. ABSTRACT	c. THIS PAGE			LEYVA, IVETT
Unclassified	Unclassified	Unclassified	UU		19b. TELEPHONE NUMBER *(Include area code)* 703-696-8478

Standard Form 298 (Rev. 8/98)
Prescribed by ANSI Std. Z39.18